A Digital Non-Foster Fast-Wave Line Using an Internet of Things Approach for Software Tuning of Multiple Digital Negative Capacitors

Kathryn L. Smith, J. Luke Stuemke, Ryan S. Adams, and Thomas P. Weldon
Department of Electrical and Computer Engineering
University of North Carolina at Charlotte
Charlotte, NC, USA
tpweldon@uncc.edu

***Abstract*—A software-tunable digital non-Foster fast-wave transmission line is presented, using an Internet of Things approach to implement tuning and signal monitoring. Such non-Foster fast-wave lines offer greater bandwidth than conventional passive designs, and a digital non-Foster approach is proposed to provide a software-adjustable implementation of the required negative capacitors. Further, an IoT (Internet-of-Things) approach is employed, where multiple non-Foster circuit elements are controlled over Ethernet by a laptop graphical user interface, including remote signal monitoring. This IoT approach has the advantage of being readily extended to accommodate more devices or multidimensional arrays. Measured data is presented for an IoT-based prototype of a superluminal digital non-Foster fast-wave line with software-tunable negative capacitance.**

I. Introduction

Fast-wave transmission lines support superluminal propagation and have important applications in leaky wave antennas [1] and cloaking [2]. Although conventional passive implementations of fast-wave lines have limited bandwidth, the bandwidth can be improved by using non-Foster circuits such as negative capacitors [3] More recently, software-adjustable fast-wave lines have been realized using digital non-Foster circuits to implement negative capacitance, where a one-dimensional array of these digital circuits are tuned in software [4], [5]. However, prior work has not addressed development of a complete system, where an array of multiple digital non-Foster elements are controlled within an IoT (Internet-of-Things) framework. Furthermore, the demonstration of an IoT-controlled one-dimensional digital non-Foster array is an important first step toward more complex systems, such as IoT-controlled two-dimensional arrays to support mantle-cloak applications [2], and other similar systems requiring multiple tunable reactive elements [4], [6]–[8].

Therefore, the present effort extends prior results by adding an Ethernet interface to digital non-Foster circuits, to provide remote control capability, to take advantage of innate software-tunability, and to add remote signal monitoring. Furthermore, a laptop-based GUI (graphical user interface) controller/monitor is developed, providing a complete client-server based system within an IoT-based framework.

978–1–5386–1539–3/17/$31.00

In [4], digital non-Foster circuits were used to provide an array of three user-programmable reactive loads for a fast-wave line, but each of the digital circuits had to be programmed individually. Because these elements are digitally implemented, they lend themselves naturally to Internet-based control. As described in [9], the Internet of Things includes devices that "can be controlled remotely and can act as physical access points to Internet services." Such Internet-based control has been used in similar systems such as antenna clusters [10], [11]. Therefore, the present work builds upon earlier digital non-Foster fast-wave results by incorporating an IoT approach to demonstrate control, tuning, and monitoring of a three-element digital non-Foster fast-wave line. In the proposed approach, a laptop-based GUI provides client-server based control of a fast-wave line within an IoT framework, where each digital non-Foster element has a unique local Ethernet address and interface.

In the following section, the theory of digital non-Foster circuits is reviewed, and the digital non-Foster fast-wave line is described in detail. In Section II-B, the IoT interface for control and tuning is described. Finally, Section III provides measured data for a 3-element prototype IoT-controlled fast-wave line.

II. IoT-Based Digital Non-Foster Fast Line

The block diagram of the overall proposed IoT-controlled fast-wave line system is shown in Fig. 1. For purposes of demonstration, a router and local Ethernet network provides communication between a laptop server and three FRDM-K64F MCU (microcontroller unit) boards. The MCU boards implement the three client-side tunable digital negative capacitors illustrated at the bottom of Fig. 1. These three negative capacitances load 91.5 meters of RG-147 coaxial line, forming a fast-wave line [3], [4]. The following subsection first reviews design of the fast-wave line and digital non-Foster elements; the subsequent subsection addresses IoT aspects of the design.

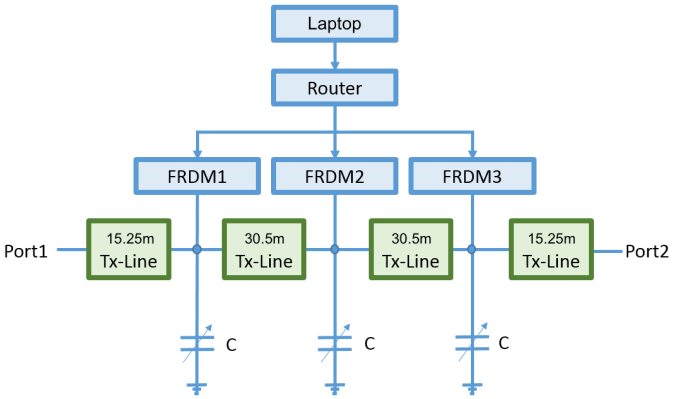

Fig. 1. Digital non-Foster fast-wave line system block diagram, including loaded transmission line. Each variable capacitor is an MCU implementation of a digital non-Foster software-adjustable negative capacitor.

A. Digital Non-Foster Fast-Wave Line

As presented in [4], [5], the general form of a digital non-Foster circuit element for the fast-wave line negative capacitors is shown in Fig. 2. The digital non-Foster circuit element is shown in the dashed box, where voltage v_{in} is digitized by the ADC (analog-to-digital converter) with period T to form discrete-time signal $v_{in}[n] = v_{in}(nT)$. The filter with z-transform $H(z)$ generates the DAC (digital-to-analog converter) drive signal. Also shown are provision to model latency (due to computation and conversion time) and two external resistors to improve capacitor quality factor and stability.

For the negative capacitance needed in Fig. 1, the required difference equation is given by [12]

$$v_{dac}[n] = \frac{(T - R_{dac}C)}{T} v_{in}[n] + \frac{R_{dac}C}{T} v_{in}[n-1] \,, \quad (1)$$

where T is the clock period, R_{dac} is the value of the resistor connected between the ADC input and DAC output pins, and C is the desired capacitance value (positive or negative). The corresponding transfer function is then:

$$H(z) = [(T - R_{dac}C)z + R_{dac}C]/(Tz) \,. \quad (2)$$

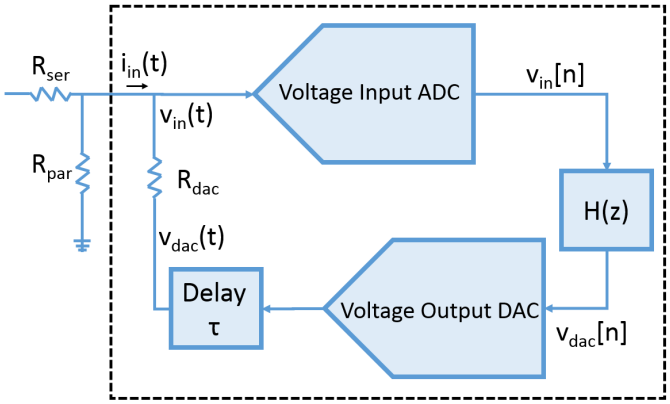

Fig. 2. Block diagram of digital non-Foster negative capacitors for use in the fast-wave line [4], [5]. The ADC digitizes $v_{in}(t)$, and the output of filter $H(z)$ drives the DAC, creating current i_{in} through R_{dac}, with latency τ.

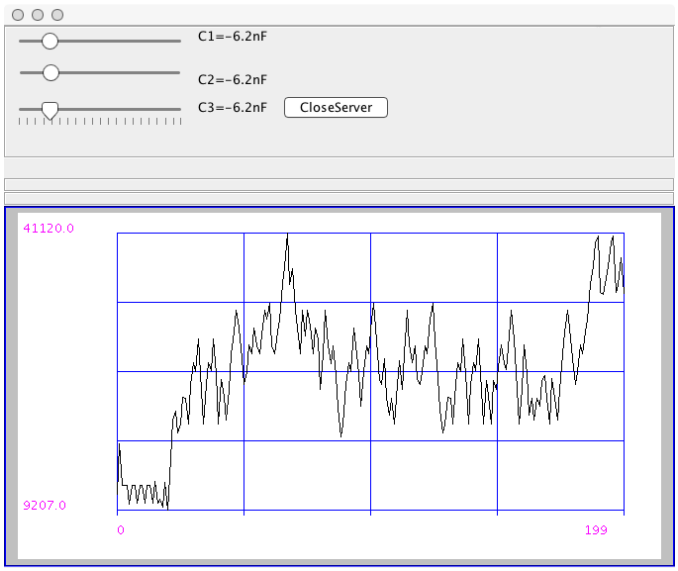

Fig. 3. Laptop server-side GUI showing a snapshot of time domain signal from ADC of one MCU, with the three sliders used to adjust the capacitance values of the three MCUs shown at the top.

The input impedance of the digital non-Foster circuit element looking into the dashed box of Fig. 2 is then [12]

$$Z(s) \approx \left. \frac{sTR_{dac}}{sT - H(z)\,(1 - z^{-1})\,e^{-s\tau}} \right|_{z=e^{sT}} . \quad (3)$$

Finally, two external resistors R_{ser} and R_{par} were added for Q-enhancement and stability, as shown in Fig. 2, which results in a total impedance

$$Z_{tot}(s) = R_{ser} + R_{par}||Z(s) \quad (4)$$

where R_{ser} is the value of the external series resistor, and R_{par} is the value of the external parallel resistor, as shown in Fig. 2.

Though much of the foregoing theory is found in [4], [5], the following subsection discusses the important novel extension of prior results to include client-server Ethernet-based tuning, monitoring, and control using an IoT framework.

B. IoT Control and Interface

System control was provided via a NetBeans GUI running on a laptop, illustrated in Fig. 3. The GUI consisted of three sliders, each of which controlled the capacitance value for one of the three MCU boards. The possible inputs for each slider ranged from -10 nF to 0 nF in increments of 0.1 nF. Each of the three MCUs was implemented as a client, and the laptop, communicating via Ethernet, was used as the server. Finally, a display area at the bottom of the GUI provides monitoring of the fast-wave line signal by displaying 200 points of the sampled ADC signal from the MCU board.

Fig. 4 shows the system software flowchart governing the interactions between the laptop server-side GUI activities and the client-side activities on each MCU. On the client side, the first step in the process is to initialize the Ethernet connection between the GUI and the three MCUs. The next step is for each MCU client to send a request to the laptop server to

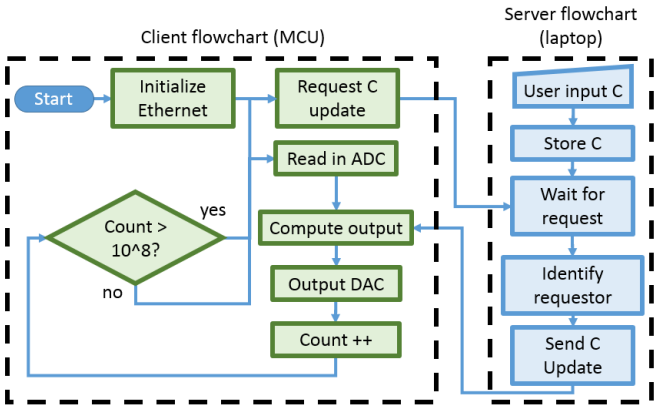

Fig. 4. System software flowchart. Left side is MCU client software flowchart for software implemented for each MCU (green for client-side activities on the MCU). Right side is laptop server flowchart (blue for the server-side activities on the laptop).

obtain the user-entered capacitance values from the laptop server/GUI. The remaining MCU client steps read the ADC, compute the filtering process $H(z)$, and set the DAC output to implement the desired negative capacitance on the board using (1). Finally, a loop count of 10^8 is used to interrupt MCU client processing approximately once every 100 seconds to request an updated C value from the server.

On the laptop server side, the first step in Fig. 4 is to accept and store the user input capacitance values from the three sliders, then wait for a request from any MCU client. Upon receipt of a request, the server first identifies the particular MCU based on Ethernet address of the incoming request. It then uses that address to send the appropriate capacitance value to the corresponding MCU board.

III. Measurement

A prototype of the overall system of Fig. 1 was built and tested as illustrated in Fig. 5. The laptop at the top of the figure acts as the server on the local network of the router, and runs the server GUI of Fig. 3. The server communicates with the three MCU boards over the local network through the Ethernet router. The three MCUs are also connected to the 91.5 m of transmission line at the bottom of Fig. 5, at the distance

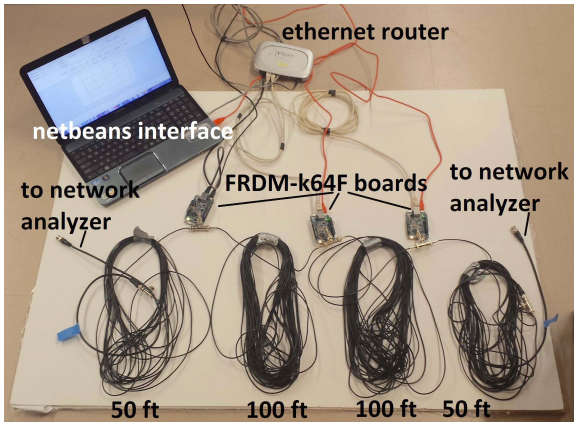

Fig. 5. Measured prototype configuration: fast wave line with IoT-based digital non-Foster loading.

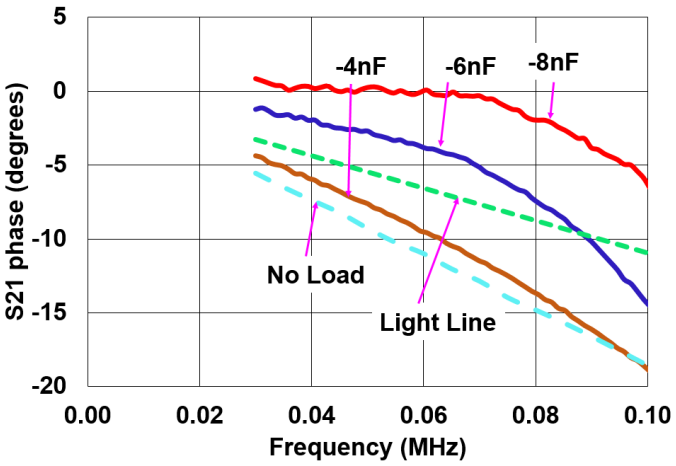

Fig. 6. Three cases of measured S_{21} phase for fast wave line with Internet-connected digital non-Foster loads programmed to -4 nF, -6 nF, and -8 nF. Also shown are the phase plots for the unloaded line (dashed cyan) and for a signal traveling at the speed of light in a vacuum (dashed green).

intervals given in Fig. 1. For the following, the parameters used to program the MCU according to (1) were set to $T = 1$ μs, $R_{dac} = 1000$ Ω, $R_{ser} = 50$ Ω and $R_{par} = 4700$ Ω.

The phase of the fast-wave line was measured first, since the phase indicates whether the desired superluminal behavior is achieved. In addition, all three capacitors loading the fast-wave transmission line were simultaneously set to -4 nF, -6 nF, and -8 nF to demonstrate control over Ethernet. Fig. 6 shows the phase of S-parameter S_{21} measured between Port 1 and Port 2 of Fig. 1, for -4 nF, -6 nF, and -8 nF tuning. Also shown are the phase plots for the unloaded line (dashed cyan) and for a theoretical transmission line having the phase velocity of light in a vacuum (dashed green). The trend of increasingly negative loading capacitance has the desired effect of reducing the magnitude of the phase of S_{21}. Superluminal phase velocity is clearly observed (phase above the "light line") for two of the three measurements (-6 nF and -8 nF), with superluminal effects decreasing near 100 kHz for all cases.

Fig. 7 shows the corresponding magnitude of S-parameters S_{11} and S_{21} measured between Port 1 and Port 2 of Fig. 1,

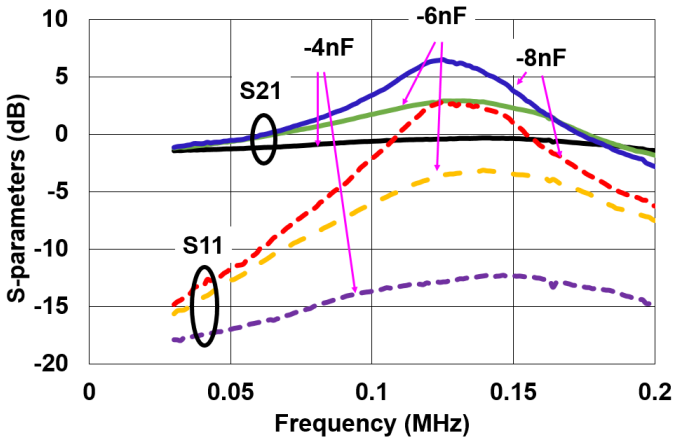

Fig. 7. Three cases of measured $|S_{11}|$ and $|S_{21}|$ for fast wave line with Internet-connected digital non-Foster loads programmed to -4 nF, -6 nF, and -8 nF.

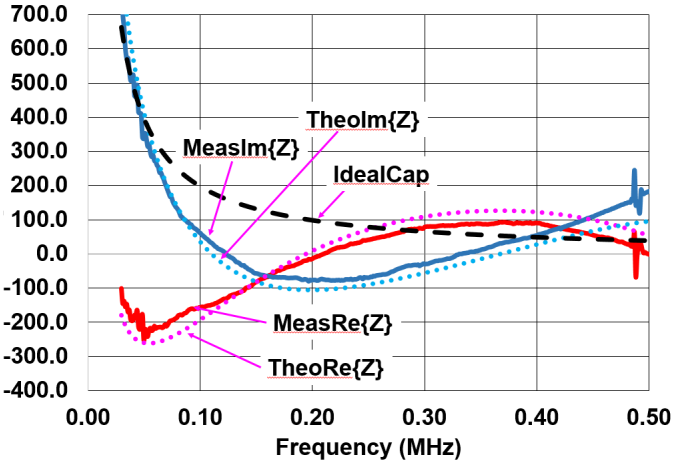

Fig. 8. Measured and theoretical input impedance Z_{tot} for a single non-Foster circuit element, for the case where $C = -8$ nF, $T = 1$ μs, $R_{dac} = 1000$ Ω, $R_s = 50$ Ω, and $R_p = 4700$ Ω. Also shown, in dashed black, is the reactance of an ideal capacitor.

again for -4 nF, -6 nF, and -8 nF. As shown, a peak in $|S_{11}|$ and $|S_{21}|$ is observed for all loading values around 125 kHz, qualitatively similar to results in [3]–[5]. Gain caused by the negative resistance (later shown in Fig. 8) is observed in the system at frequencies near this peak.

Finally, the performance of each of the three digital non-Foster circuits was measured. Each of three MCUs was programmed as discussed, with the client side protocol outlined in Fig. 4. The measured input impedance Z_{tot} to a single non-Foster circuit element of Fig. 2 programmed to a capacitance of -8 nF, including external stabilizing resistors R_{ser} and R_{par}, is shown in Fig. 8. As shown, both the real and the imaginary parts of the impedance match the theoretical results from (4) very well across the measured spectrum. The imaginary part of the impedance matches the impedance of an ideal negative -8 nF capacitor below approximately 50 kHz. The measured and theoretical magnitude of Q-factor, $Q = |Im\{Z\}/Re\{Z\}|$, of a single non-Foster circuit element of Fig. 2 programmed to a capacitance of -8 nF is shown in Fig. 9. This figure also shows the effect of the stabilizing resistors on the quality factor of the implemented capacitance. Because the real part of the impedance is largely negative at low frequencies (as shown in Fig. 8), the externally added positive resistance has the effect of increasing the Q-factor and improving performance of the fast-wave line. The Q-factor for the case including the external resistors is above 2 up to approximately 50 kHz.

IV. Conclusion

Three stable software-tunable digital negative capacitors have been implemented in a fast-wave transmission line. Superluminal phase velocity, with tunability provided over Ethernet, has been demonstrated. The measured data are in agreement with prior results in [4], [13], [14], but with the new added advantage of Ethernet connectivity, which allows the phase velocity of the loaded transmission line to be dynamically reprogrammed remotely, and allows simple expansion for systems or arrays that may include more devices.

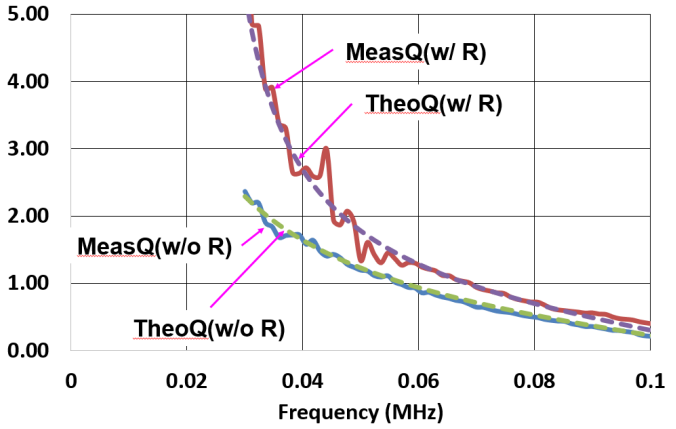

Fig. 9. Measured and theoretical Q-factor for a single digital non-Foster circuit without external loading resistors, shown in solid blue and dashed green, and with external resistors, shown in solid red and dashed purple.

Since the non-Foster approach is a digital implementation, the circuit performance should also be readily scalable to higher clock frequencies in more advanced processes. This could enable new non-Foster applications requiring numerous elements such as superluminal lines for antenna arrays, unit cells, two-dimensional mantle cloaks, and unit cells in three-dimensional metamaterials. In addition, the tunable aspects of the proposed digital design allow variation of parameters through such arrays.

Acknowledgment

This material is based upon work supported by the National Science Foundation under Grant No. DGE-1439650.

References

[1] W. Menzel, "Planar leaky-wave antennas - early concepts and actual results," in *Microwave Conference (EuMC), 2013 European*, Oct. 2013, pp. 483–486.

[2] P.-Y. Chen, C. Argyropoulos, and A. Alù, "Broadening the cloaking bandwidth with non-Foster metasurfaces," *Phys. Rev. Lett.*, vol. 111, pp. 233 001:1–5, Dec. 2013.

[3] J. Long, M. Jacob, and D. Sievenpiper, "Broadband fast-wave propagation in a non-Foster circuit loaded waveguide," *IEEE Trans. Microw. Theory Techn.*, vol. 62, no. 4, pp. 789–798, Apr. 2014.

[4] K. Smith, R. Adams, and T. Weldon, "Measurement of a fast-wave line using digital non-Foster circuits for software-adjustable delay," in *2016 IEEE Antennas and Propagation Society International Symposium (APSURSI)*, June. 2016.

[5] T. P. Weldon and R. S. Adams, "A digital discrete-time non-Foster approach to broadband fast-wave microstrip lines," in *Advanced Electromagnetic Materials in Microwaves and Optics (METAMATERIALS), 2015 9th International Congress on*, Sep. 2015, pp. 322–324.

[6] N. Honma, T. Seki, K. Nishikawa, and K. Tsunekawa, "Series-fed beam-scanning array antenna comprising multi-stage configured microstrip antenna with tunable reactance devices and open stubs," in *Antennas and Propagation Society International Symposium, 2004. IEEE*, vol. 4, June 2004, pp. 3980–3983 Vol.4.

[7] N. Yang, C. Caloz, and K. Wu, "Fixed-beam frequency-tunable phase-reversal coplanar stripline antenna array," *IEEE Transactions on Antennas and Propagation*, vol. 57, no. 3, pp. 671–681, March 2009.

[8] Y. K. Jung and B. Lee, "Beam scannable patch array antenna employing tunable metamaterial phase shifter," in *Proceedings of the 2012 IEEE International Symposium on Antennas and Propagation*, July 2012, pp. 1–2.

[9] F. Mattern and C. Floerkemeier, "From active data management to event-based systems and more," K. Sachs, I. Petrov, and P. Guerrero, Eds. Berlin, Heidelberg: Springer-Verlag, 2010, ch. From the Internet of Computers to the Internet of Things, pp. 242–259. [Online]. Available: http://dl.acm.org/citation.cfm?id=1985625.1985645

[10] S. H. Lu, Y. G. Chen, and L. C. Wang, "Antenna clustering for distributed large-scale mimo systems," in *Internet of Things (iThings), 2014 IEEE International Conference on, and Green Computing and Communications (GreenCom), IEEE and Cyber, Physical and Social Computing(CPSCom), IEEE*, Sept 2014, pp. 578–582.

[11] W. Amasiri, S. Lerdnantawat, and D. Bunnjaweht, "An internet-based coaxial switching system for an amateur radio station with multiple antennas," in *2015 7th International Conference on Information Technology and Electrical Engineering (ICITEE)*, Oct 2015, pp. 322–325.

[12] P. J. Kehoe, K. K. Steer, and T. P. Weldon, "Thevenin forms of digital discrete-time non-Foster RC and RL circuits," in *2016 IEEE Antennas and Propagation Society International Symposium (APSURSI)*, Jul. 2016, pp. 1–2.

[13] T. P. Weldon, J. M. C. Covington, K. L. Smith, and R. S. Adams, "Performance of digital discrete-time implementations of non-foster circuit elements," in *2015 IEEE International Symposium on Circuits and Systems (ISCAS)*, May 2015, pp. 2169–2172.

[14] T. P. Weldon, J. M. C. Covington, K. L. Smith, and R. S. Adams, "Stability conditions for a digital discrete-time non-foster circuit element," in *2015 IEEE International Symposium on Antennas and Propagation USNC/URSI National Radio Science Meeting*, July 2015, pp. 71–72.